IAC-12-A6.2.6

ATTITUDE MOTION OF SPACE DEBRIS OBJECTS UNDER INFLUENCE OF SOLAR RADIATION PRESSURE AND GRAVITY

Carolin Früh
University of New Mexico, USA, cfrueh@unm.edu

Thomas Schildknecht
University of Bern, Switzerland, thomas.schildknecht@aiub.unibe.ch

Space debris objects are resident space objects, which are neither actively nor passively controlled any more. Those objects either are not any more, or either never have been in a controlled orbital or attitude state. In near geostationary orbits, the main sources of forces acting on the body are Earth and third body gravity field, solar radiation pressure. Via optical observations astrometric positions and velocities may be determined. Furthermore, light curves, brightness measurements over time, may be determined. Those light curves are a superposition of the lighting geometry, shape of the object and its attitude motion. In this paper, two kinds of space debris objects are investigated. First, an upper stage, which have a significant offset between the geometrical center and the center of mass after burning up the contained fuel, which leads to a significant attitude motion. Secondly, high area-to-mass ratio (HAMR) objects in near geostationary orbits are investigated. Those objects, which were initially detected by Schildknecht in 2004, are extremely light objects, which are most sensitive to orbital as well as attitude perturbations. Whereas in the case of the upper stage shape and materials of the objects are in general known, the shape of HAMR objects in unknown. MLI is a likely candidate for the material of those objects. In this paper the assumption of a flat rigid sheet is used.
The coupled orbit and attitude dynamics of those three object classes are studied and light curves are simulated. Those simulated light curves are compared to actually measured light curves, obtained with the one meter ZIMLAT telescope, located in Bern, Switzerland.

I. INTRODUCTION

Since the launch of the first satellite Sputnik in 1956, space has become populated with more and more space resident objects. Whereas about 20 000 objects are regularly tracked by the US Space Command, statistical measurements suggest a population of over 300 000 objects in near Earth space. Only about 7 percent of the resident space objects are active space assets, which may be in a controlled and communicative state. Space debris – objects with no function any more – are non-controlled objects. The majority of those objects are not identified. This has two main reasons: Whereas with ground based radars, re-solved images of large space assets in low Earth orbits can be obtained [1], this is not possible for small objects. No resolved images can be gained of objects, which are in higher altitude orbits, e.g. close to the geostationary ring, using ground based optical sensors. Secondly, objects which are followed up with observations and kept in catalog for a certain amount of time, may be lost after a while, due to scarce sensor resources and insufficient dynamical modeling of the orbital and, if significant, attitude evolution.

The astrometric places of near GEO objects can readily be extracted from non-resolved optical images, and allow the determination of a first orbit. Follow-up

observations can be used to improve a first orbit [2]. If the object is cataloged in an orbital element catalog, and covariances are small enough for a unique association, this may be sufficient for a successful object identification. But if the object is not cataloged or covariances overlap, as it is the case in dense regions, as satellite clusters e.g., orbital information alone is not sufficient. Light curves measure the variation of the brightness of the object over time. The brightness of the object is determined by the lighting and viewing geometry, the shape, reflection properties and attitude motion of the object. In general, the lighting and viewing geometry is known. In absence of knowledge about the exact object properties and attitude motion, light curves can never be unique [3].

The orbit and attitude are subject to perturbations, for objects in near geostationary orbits, the main perturbations are caused by Earth and third body gravitational fields, and solar radiation pressure. Orbital and attitude dynamics are coupled. The effects of that coupling are especially prominent for objects with high area-to-mass ratios (HAMR), as they were detected by T. Schildknecht in 2004 [4, 5]. Neglecting the attitude motion in the orbit propagation can lead to significant offsets between the propagated and the true state of an object [6, 7], which can prevent a successful re-detection. But also other objects, like upper stages, which have a significant offset between the geometric center and the center of mass have significant attitude motion, due to a change in attitude motion. Even when shape and reflection properties are unaltered, the signatures in the light curves are subject to change over time, even when measured under the same lighting and viewing conditions. This prevents a simplistic fingerprinting via light curves to enhance existing orbital element catalogues. Studies suggest that using several a priori shape models in an estimation process ruling out several unrealistic shapes in object identification [8].

In the present paper, the measured light curves are compared to light curves, which are generated using simplified shape models and reflection properties under realistic orbit and attitude propagation. The light curves of one upper stage, which is simplified as a cylindrical shape, are investigated, as well as of two HAMR objects, which are approximated as flat rigid sheets. The observations have been gained with the one meter Zimmerwald Laser and Astrometry Telescope (ZIMLAT) located close to Bern, Switzerland. The orbital elements are taken from two line elements for the catalogued objects and the internal orbital elements of the catalog of the Astronomical Institute of the University of Bern for the HAMR objects. The objects in the catalog have been followed and monitored over several years.

II. MEASURED LIGHT CURVES

The measured light curves were gained using the one meter ZIMLAT telescope, operated by the Astronomical Institute of the University of Bern. The measurements have been taken with a subframe technique, imaging only the object itself and the adjacent pixels to speed up readout time. This has the advantage to allow a very rapid sampling in the range of two to three seconds. The subframes are accompanied with mapping series. Those are used to determine absolute external error in determined magnitudes in comparison with the star catalog Tycho (TYC) supplemented by USNO 2B. For the short series, spanning a few minutes, normally one mapping series is taken, which leads to the assumption of identical magnitude errors for all or a number of brightness measurements in a series. Internal magnitude errors are determined using the signal to noise ratios of the individual measurements.

The light curves have been analyzed. At first a Fast Fourier transformation was applied. The Fourier transformations

revealed very short periods. On the other hand, it is a known deficiency that Fourier transformations cannot reveal periods in the order of magnitudes of the measurement interval. In addition, a time series analysis has been done with using two different power spectral density methods. The periodogram method [9], and Welch's method [10], which divides the signal in overlapping segments, and averages the modified periodograms of each segment and scales it.

The light curves of one upper stage and two objects with high area-to-mass ratio (HAMR) have been measured. The object properties are listed in Tab.1. The details of the light curve measurements are listed in Tab.2.

The object with the COSPAR number 1988-034D, is a Block DM-2 upper stage. Lanched at 26th of April in 1988, at Baikonur, the upper stage was used for a Proton K rocket, employing Kosmos 1940 satellite. It has a gross mass 17,300 kg, unfueled a mass of 2,300 kg. The upper stage itself has a complex inner structure, but when employed their shape may be well approximated by a cylindrical shape. The properties of the object are listed in Tab.1. Fig.1 shows two light curves which where measured in April 2008, separated by 12 days, both times the observation started shortly before midnight. The object is in a geostationary transfer orbit and was observed close to apogee both times. Details on the observation of the light curves are listed in Tab.2.

Furthermore, objects with high area-to-mass ratios (HAMR) have been observed. HAMR have first been detected in 2004 by T. Schildknecht [4, 5]. Those objects are extremely sensitive to orbital perturbations. It is suspected that they are multi layer insulation (MLI) materials. Two objects of the internal catalog of the Astronomical Institute of the University of Bern (AIUB) have been selected, with the inter-

object	COSPAR	launch date	site	shape	size	mass	gravity offset	suspected motion
Block DM-2	1988-034D	1988-4-26	Baikonur	cylindrical	h=7.10, dia=3.70	2300	≈ 0.21	tumbling

Table 1: Object data: Name, COSPAR number, launch date, launch site, shape, size in meters, unfuelled mass in kilogram, offset between geometric center and center of mass of the object in meter, and suspected motion [11, 13, 14].
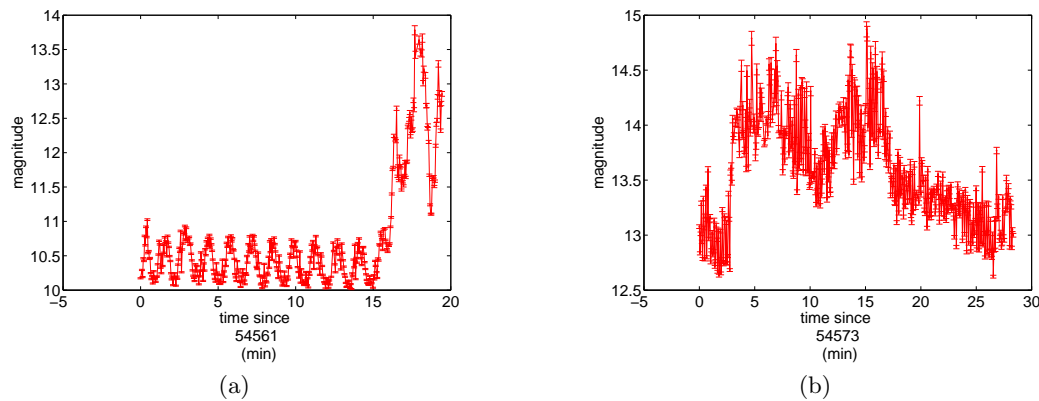
(a)   (b)

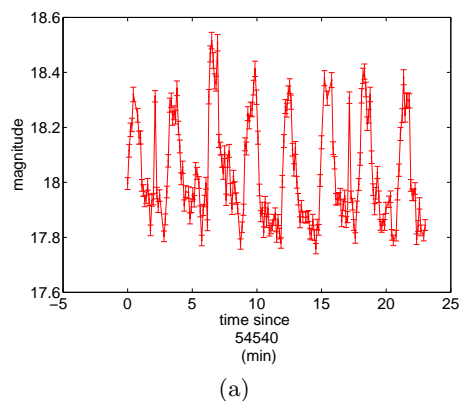Figure 1: Light curves of Block DM-2 1988-034D.

(a)

Figure 2: Light curve of HAMR object E07337C.

nal names E07337C and E07047A. Those objects are not listed in any other publicly available catalog and do not have COSPAR numbers, consequently. No information on material, size, shape, attitude or origin are available so far. Tab.2 lists the information on the observed light curves of both objects. The light curves are displayed in Fig.2 and 3, respectively.

III. SIMULATED LIGHT CURVES

A comparison of the measured light curves with simulated ones have been done. In the simulation setup the osculating elements 30 min to one hour prior to the start epoch of the light curves are used, as well as the extracted main periods are used to simulate rotations around the main axis of inertia. In the simulation the orbit and attitude motion are integrated in a fully coupled system over the time interval, in which the light

curve was measured. For objects, for which several light curves are measured within the same night, the orbit attitude motion is integrated over the whole night. Geocentric equations of the orbital motion read as:

$$\ddot{\vec{x}} = -GM_\oplus \nabla V(\vec{x}) -$$
$$G \sum_{k=1,2} M_k \left[\frac{\vec{x} - \vec{x}_k}{|\vec{x} - \vec{x}_k|^3} + \frac{\vec{x}_k}{x_k^3} \right] + \sum_l \vec{a}_l$$

where $\vec{x}$ is the geocentric position and velocity vector of the object, G the gravitational constant, $M_\oplus$ the Earth mass and $V(\vec{x})$ the Earth gravitational potential, which has been taken into account to order and degree six, third body perturbations of Sun and Moon (k=1,2) are taking into account as well as radiation pressure as acceleration causing orbital perturbation. The dynamic equations of motion a rigid body can be calculated using Euler's equations:

$$\frac{d}{dt}(I\vec{\omega}) = \sum_{l=1}^{h} \vec{\tau}_l - \vec{\omega} \times (I\vec{\omega}), \qquad (1)$$

$$I_{\alpha\beta} = \sum_{k=1}^{n} m_k (r_k^2 \delta_{\alpha\beta} - z_{k,\alpha} z_{k,\beta}),$$

$$r_k = \sqrt{\sum_{\alpha,\beta,\gamma} z_k^2}$$

where $\vec{\omega}(t)$ the angular velocity body rate. $I_{\alpha\beta}$ is the net tensor of the moments of inertia, with mass m_k located at position $z_{\alpha\beta\gamma}$, δ is the Kronecker delta. $\sum_l \vec{\tau}_l$ represents the sum of the h disturbance torques. For the kinematic equations, quaternion repre-
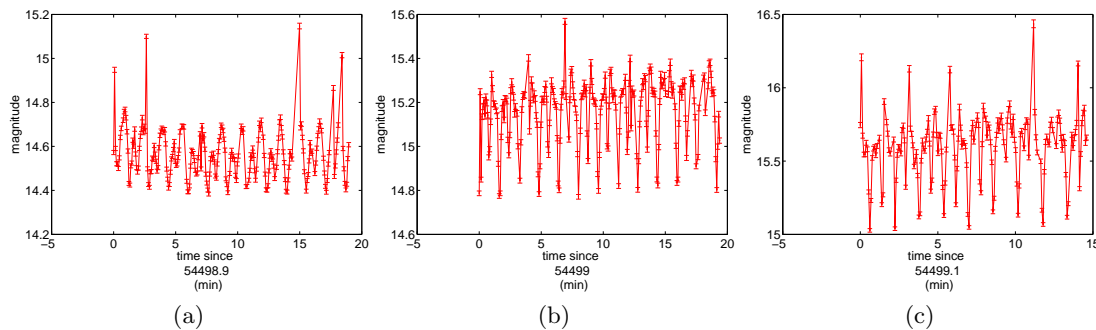
Figure 3: Light curves of HAMR object E07047A.

sentation is used:

$$\frac{d\vec{q}}{dt} = 0.5 \cdot \Omega \cdot \vec{q} \qquad (2)$$

$$\Omega = \begin{bmatrix} 0 & \omega_3 & -\omega_2 & \omega_1 \\ -\omega_3 & 0 & \omega_1 & \omega_2 \\ \omega_2 & -\omega_1 & 0 & \omega_3 \\ -\omega_1 & -\omega_2 & -\omega_3 & 0 \end{bmatrix}$$

No controll torques are present. The gravitational torque is simulated:

$$\vec{\tau}_{\mathrm{grav}} = \frac{GM}{\xi^2} \left[m(\hat{\vec{\xi}} + \vec{\rho}_{\mathrm{grav}}) + \frac{3}{\xi}(\hat{\vec{\xi}} \times (I\hat{\vec{\xi}})) \right] \quad (3)$$

where $\hat{\vec{\xi}} = A_{cos} \cdot \hat{\vec{x}}$ is the position vector of the object transformed to the body system by the inertial to body transformation matrix A_{cos}, G is the gravitational constant, $M_\oplus$ the mass of the Earth, $m = \sum_k m_k$ the total mass of the object, $\vec{\rho}_{\mathrm{grav}}$ is center of mass relative to the geometric center in the body reference frame.

The radiation force, affecting orbit and attitude (the latter in case of extended HAMR objects and at shadow pathes even for objects with uniform reflection properties [6]), is determined for flat surfaces as the following [17]:

$$\vec{F}_{\mathrm{rad}} = -\frac{A}{m}\frac{E}{c}\frac{A_\oplus}{|\vec{x} - \vec{x}_\odot|^2} \cdot P(\hat{\vec{S}}) \qquad (4)$$

for $0 < \arccos(\hat{\vec{S}}\hat{\vec{N}}) < \pi/2$. m is the total mass of the object, E is the solar constant, $A_\oplus^2$ the astronomical unit, $\vec{x}_\odot$ the geocentric position of the sun, c velocity of light, $\vec{S}$ the direction of the radiation source, A is the area of the illuminated surface. $\vec{x}$ is the position vector to the center of pressure of the surface. For flat surfaces function P it is determined as the following:

$$P = \hat{\vec{S}}\hat{\vec{N}}[(1 - C_{\mathrm{s}})\hat{\vec{S}} + 2(C_{\mathrm{s}} \cdot \hat{\vec{S}}\hat{\vec{N}} + \frac{1}{3}C_{\mathrm{d}})\hat{\vec{N}}] \quad (5)$$
$$C_{\mathrm{s}} + C_{\mathrm{d}} = 1 - C_{\mathrm{a}}$$

$C_{\mathrm{s,d,a}}$ are the coefficients for specular, diffuse reflection and absorption, and $\hat{\vec{N}}$ the normal vector of it for a flat surface. For the cylinder barrel of area $A = 2rh$,with radius r and height h, and symmetry axis $\vec{N}$, P is defined as:

$$P = [(1 + \frac{1}{3}C_{\mathrm{s}})\sin(\phi) + \frac{\pi}{6}C_{\mathrm{d}}] \cdot \hat{\vec{S}} +$$
$$(-\frac{4}{3}C_{\mathrm{s}}\sin(\phi) - \frac{\pi}{6}C_{\mathrm{d}}) \cdot \cos(\phi) \cdot \hat{\vec{N}} \quad (6)$$

ϕ is the angle measured from the sun direction to the symmetry axis of the cylinder. The light curves of the objects are simulated. The magnitude theoretically measured by a ground based sensor (neglecting atmosphere), is determined as the following:

$$\mathrm{mag} = \mathrm{mag}_\odot - 2.5 \log\left(\frac{A}{\pi \cdot x^2}G(\hat{\vec{O}}, \hat{\vec{S}})\right). \quad (7)$$

The quantity $\mathrm{mag}_\odot$ is the magnitude of the sun, $\vec{O}$ the direction from the sensor to the object, $G(\hat{\vec{O}}, \hat{\vec{S}})$ is the reflection function. A is the area of the illuminated area. For flat facets the reflection function is defined as:

$$G = \hat{\vec{N}}\hat{\vec{S}}\left[C_{\mathrm{d}}\hat{\vec{O}}\hat{\vec{N}} + \frac{\gamma \cdot C_{\mathrm{s}} \cdot x_\odot^2}{R_\odot^2}\right], \quad (8)$$

$$\gamma = \begin{cases} 1 & \text{for } \cos(0.25\,\mathrm{deg}) \leqslant \frac{\vec{O}+\vec{S}}{|\vec{O}+\vec{S}|} \cdot \hat{\vec{N}} \\ 0 & \text{else} \end{cases}$$

object	COSPAR	start epoch	int. (min)	phase (deg)	a (km)	e	i (deg)	er. mag.	periods F/W/Per (min)
Block DM-2	1988-034D	04-Apr-08 23:49	20	62.1 - 57.1	42212	0.002	12.27	0.61	1.2 / 9,8 0.9 / 3.3 12.8
Block DM-2	1988-034D	16-Apr-08 23:34	28	73.0 - 65.9	42214	0.002	12.29	0.32	2.0 4.8 / 0.6 9.8 / 2.4 25.6
E07337C	-	15-Mar-08 00:14	23	16.4 - 11.8	42429	0.055	14.31	0.22	1.0 4.8/ 1.0 9.3 / 2.1 16.0
E07047A	-	02-Feb-08 22:38	19	17.1 - 17.9	39981	0.194	12.58	1.31	0.4 0.7/ 1.4 9.3/ 0.9 8.3
E07047A	-	03-Feb-08 00:52	20	32.0 - 35.2	39981	0.194	12.58	1.31	0.8 1.0/ 0.9 8.3 / 1.0 8.3
E07047A	-	03-Feb-08 02:11	15	45.8 - 48.5	39981	0.194	12.58	1.31	0.4 0.7/ 0.7 8.3 / 3.0 16.0

Table 2: Measured light curves: Object, COSPAR number, start epoch of the measurement (UTC), duration of the measurement in minutes, phase angle in degree, semi-major axis in kilometers, inclination in degree, error of the absolute measured magnitude, dominant periods determined in the light curve in minutes, Fast Fourier Transformation, Power Spectral Density: Welch, Periodicy method.

where $0 < \arccos(\hat{\vec{S}}\hat{\vec{O}}) < \pi/2$. γ is the specular reflection parameter. The dimension of the sun has been taken into account, where $R_\odot$ is the radius of the Sun, $x_\odot$ is the distance from the object to the Sun. No limb darkening effects have been accounted for. For the cylinder barrel, with $A = 2rh$, we get the following reflection function:

$$G = \sin(\psi)\sin(\omega)\left[\frac{C_\mathrm{d}}{4}\left(\sin(\theta) + \right.\right.$$
$$\left.\left.(\pi - \theta)\cos(\theta)\right) + \frac{0.5}{180.0} \cdot \frac{\gamma \cdot C_\mathrm{s} \cdot x_\odot^2}{R_\odot^2}\right] \quad (9)$$

$$\gamma = \begin{cases} 1 & \text{for } 89.75\deg \leqslant \mathrm{acos}(\frac{\vec{O}+\vec{S}}{|\vec{O}+\vec{S}|} \cdot \hat{\vec{N}}) \\ & \leqslant 90.25\deg \\ 0 & \text{else} \end{cases}$$

ψ is the angle between the sun and the symmetry axis, ω the angle between the observer and the symmetry axis in the plane containing the symmetry axis in the body fixed coordinate system. θ is the angle between the observation direction $\hat{\vec{O}}$, from the station to the object, and the direction of the sun to the object $\hat{\vec{S}}$ in the plane orthogonal to the symmetry axis of the cylinder.

IV. Results

Light curves of all observed objects have been simulated. In the simulations the lighting conditions at the exact observation epochs have been reproduced, the object shapes and rotation periods as displayed in Tab.1 and Tab.2 have been used.

The upper stage Block DM-2 has been simulated using reflection values of 0.4 for the Lambertian and 0.3 for the specular reflection, as simple cylinder shape, using the values displayed in Tab.1.The periods, displayed in Tab.2, however, do not reveal, around which axis the rotation took place and lead to the specific light curve pattern. Furthermore, only apparent rotation can be extracted. For objects near geostationary ring, no investigations of true and apparent rotation can be done. For objects Block DM-2 the motion is influenced by the significant offset between

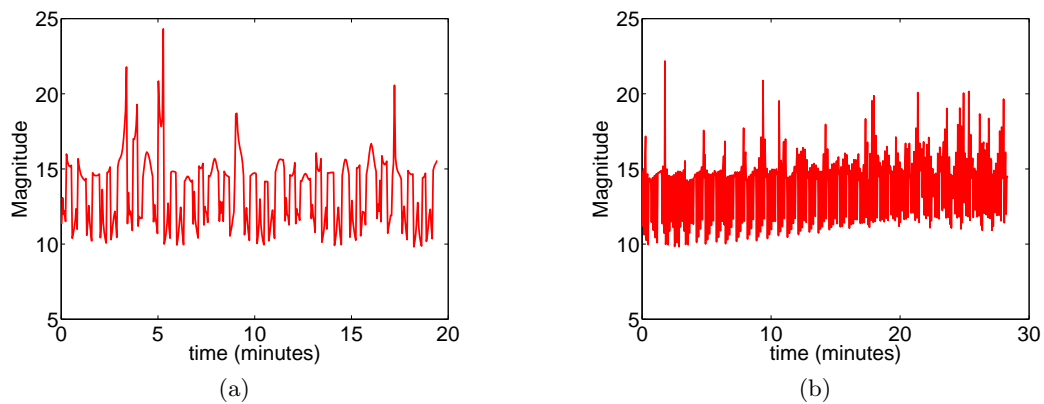(a)   (b)

Figure 4: Simulated light curves of Block DM-2 upper stage 88034D.

the geometrical center and the center of mass.

Fig.4 shows the simulated light curves of the Block DM-2 1988-034D object. The comparison of the simulation results, in Fig.4 with the measured results in Fig.1 shows, that the general trends in the second light curve have been captured correctly. In the first light curve, simulation shows a similar substructure than the first part of the measured light curve. However, the simulation does cover a larger magnitude range. The drop in magnitude at the end of the measurement is consistent with a drop in magnitude of the simulation, a couple of minutes earlier. In the second light curve, rapid brightness variations can be observed in both light curves. The long term structure of the measured light curve could not be reproduced.

The two HAMR objects have been simulated as flat surfaces with the reflection coefficients of specular reflection of 0.6 and Lambartian reflection coefficient of 0.26. The simulated light curves are displayed in Fig.5 and Fig.6. For object E07337C a size of 0.05 square meters has been assumed, for object E07047A of 0.5 square meter. The sizes have been estimated, to match the measured magnitudes with the given reflection properties. Using the periods determined in the Fourier analysis resulted in a too rapid rotation, for which the light curves did not resemble the measured ones.
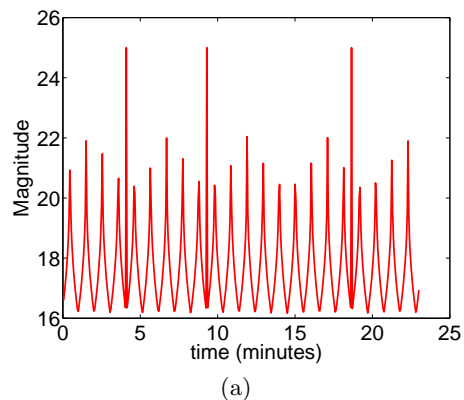

(a)

Figure 5: Simulated light curve of HAMR object E07337C.

It can be observed in both cases that the simulated light curves agree with the measured ones using periods determined with Welch's method, but are a lot more smooth than the actual measurements. In case of object E07337C, the brightness variations in the simulations are larger than in the observations, compare Fig.2 and Fig.5. In the measured light curve, Fig.2 the variations in brightness are only about one magnitude. This could mean two things, either that the smallest magnitudes cannot be observed by the telescope, and are therefore not detected. The limiting magnitude of the ZIMLAT telescope is about the 18th magnitude. Furthermore it could mean, that the attitude-shape assumption is not sufficient, meaning that either a flat plate is not resembling the true object enough or that the attitude motion is different. It could mean that the object is not performing full rotations, but
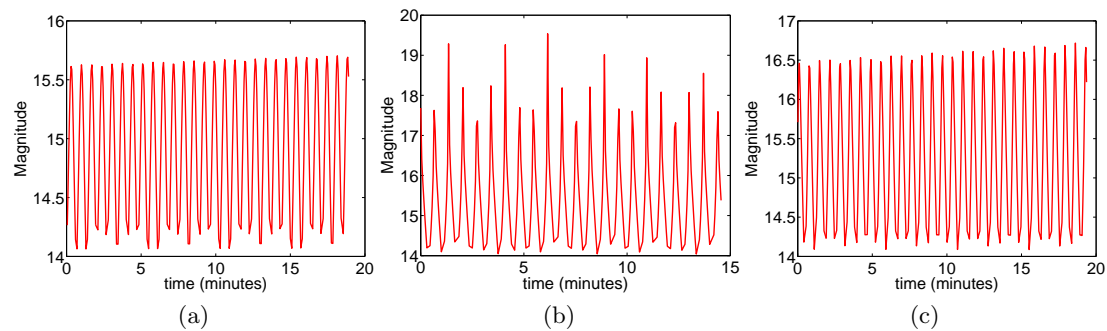
Figure 6: Simulated light curves of HAMR object E07047A.

more a pendulum motion, swinging back and forth, without ever completing a full rotation.

For object E07047A, the three simulated light curves look smoother than the measured ones. Although magnitudes in general agree, peak values are less frequent in the measured light curves. In the measured light curves smaller peaks occur with a significantly smaller variation in magnitude, those are present in the simulated light curves, but the differences in magnitude range are similar to the highest and smallest magnitudes.

V. Conclusions

The light curves have been measured of the upper stage Block DM-2 (1988-034D), as well as of two high area-to-mass ratio (HAMR) objects of the internal catalog of the Astronomical Institute of the University of Bern (AIUB).

The upper stage Block DM-2 has been simulated as cylindrical shapes, using the dimensions, that are listed in literature. The HAMR objects have been simulated as flat rigid MLI plates. For all shapes, coupled orbit attitude propagation has been used during the night, in which the light curves were measured. The attitude motion of the upper stage is significantly influenced by an offset between the geometrical center and the center of mass of the objects. Additional spin rates have been extracted from the light curves,

using Fourier transformation, periodogram method as well as Welch's method.

When comparing simulated with measured light curves, rotation periods determined with either Welch's or periodogram method produces results that resemble the measured values. However the simulated light curves are significantly smoother than the measured ones and in general cover a larger magnitude range than in the measured light curves. Good agreement can be achieved for the HAMR objects. For the upper stage, some rapid features could be reproduced, but longer periodic variations are missing in the simulations.

VI. Acknowledgments

References

[1] D. Mehrholz, L. Leushacke, W. Flury, R. Jehn, H. Klinkrad, and M. Landgraf. Detecting, Tracking and Imaging Space Debris. In *esa bulletin*, volume 109, 2002.

[2] C. Früh. *Identification of Space Debris.* Shaker Verlag, Aachen, 2011. ISBN: 978-3-8440-0516-5.

[3] H.N. Russel. On the Light-Variations of Asteroids and Sattelites. *Astrophys. J.*, 24(5):1–18, 1906.

[4] T. Schildknecht, R. Musci, M. Ploner, G. Beutler, J. Kuusela, J. de León Cruz, and L. de Fatima Domínguez Palmero. Optical Observations of Space Debris in GEO and in Highly-Eccentric Orbits. *Advances in Space Research*, 34(5):901–911, 2004.

[5] T. Schildknecht, R. Musci, M. Ploner, U. Hugentobler, M. Serra Ricart, J. de León Cruz, and L. de Fatima Domínguez Palmero. Geostationary Orbit Objects Survey. Final Report, ESA ESOC Contract 11914/96/D/IM, 2004.

[6] C. Früh, T. Kelecy, and M. Jah. Attitude Dynamics Simulation of MLI Space Debris Objects in Geosynchronous Earth Orbits. In *Proceedings of the 22th AAS/AIAA Astrodynamics Specialist Conference, Minneapolis, MN, August 13-16, 2012*, volume Minneapolis, MN, 2012.

[7] T. Kelecy and M. Jah. Analysis of Orbit Prediction Sensitivity to Thermal Emissions Acceleration Modeling for High Area-to-mass Ratio (HAMR) Objects. In *AFRL-RD-PS*, volume TP-1-1021, 2009.

[8] R. Linares, J. Crassidis, M. Jah, and H. Kim. Astrometric and Photometric Data Fusion for Resident Space Object Orbit, Attitude, and Shape Determination Via Multiple-Model Adaptive Estimation. In *AIAA Guidance, Navigation, and Control Conference 2 - 5 August 2010, Toronto, Ontario Canada*, 2010.

[9] P. Stoica and R.L. Moses. *Introduction to Spectral Analysis.* Prentice-Hall, 1997.

[10] P.D. Welch. The use of fast fourier transform for the estimation of power spectra: A method based on time averaging over short, modified periodograms. *IEEE Trans. Audio Electroacoustics*, AU-15:70–73, 1967.

[11] Mark Wade. Encyclopedia Astronautica. `www.astronautix.com`, 2012.

[12] Chris Peat, DLR/GSOC. heavens-above. `www.heavens-above.com`, 2012.

[13] US Strategic Command (USSTRATCOM). Space Track. `www.space-track.org`, 2012.

[14] Gunter Dirk Krebs. Skyrocket. `space.skyrocket.de`, 2012.

[15] European Organisation for the Exploitation of Meteorological Satellites. Eumetsat. `www.eumetsat.int`, 2012.

[16] *Mechanisms and pyros subsystem for the METEOSAT second generation.* D. Danesy. European Space Agency, ESA-SP, 438, p.169.

[17] J.R. Wertz. *Spacecraft Attitude Determination and Control.* Volume 73. D.Reidel Publishing Company, Dordrecht: Holland, 1978. ISBN: 90-277-0959-9.